Corner Features for Unifying Coordinate Systems of Multiple LIDAR Stations

Jaan-Rong Tsay
Department of Geomatics, National Cheng Kung University
1 University Rd., Tainan, TAIWAN
tsayjr@mail.ncku.edu.tw

Shu-yi Lee
Department of Geomatics, National Cheng Kung University
1 University Rd., Tainan, TAIWAN

Abstract: This paper proposes a semi-automatic method for registration of terrestrial laser point sets acquired at different stations. Firstly, a point cloud on a local plane is selected manually, and then a mathematical plane is fitted in a least squares manner onto them. Three local planes on an object corner are thus respectively determined, and their intersection point is computed by solving these three plane equations. Such points are used as tie points for transforming different laser coordinate systems into a common one. The transformation is bad in cases of inaccurate, or insufficient, or worse-distributed tie points. This paper adopts suitable "virtual corner points" to solve this problem. The test results show that suitable virtual corner points really can improve the geometrical condition for the transformation and thus raise the accuracy of corresponding transform parameters with the improvement rate of 36% to 71%. On the other hand, the ratio of the RMSD-value to the scanning distance S becomes a constant of 0.00015 in case of S ≥ 50m, where RMSD denotes the root mean square value of the perpendicular distance from a laser point to its corresponding plane.
Keywords: LIDAR, corner feature point, coordinate transformation, least squares fitting.

1. Introduction

Terrestrial laser scanner can rapidly acquire accurate and dense 3D point clouds on the surfaces of scanned objects such as buildings. The point clouds provide the detailed data necessary for an accurate building modeling or object reconstruction. In order to acquire complete laser points on a scanned building, the scanning operations must be done at more stations. Each laser scanning station has its own coordinate system representing the 3D position of each laser point. Therefore, all coordinate systems of different stations must be transformed into a common system to register surfaces implicitly expressed by those laser points acquired on different laser-scanning stations.

Different ways are available for the purpose of unifying the coordinate systems. For example, a method registers ground-based laser range images by means of those extracted line features, and thus determines the transformation parameters [1]. On the other hand, some corresponding local planes are firstly somehow found in the point sets of different laser stations, and then their normal vectors are utilized to determine the transformation parameters for those stations [2]. Also, planar or 3D targets are popular accessories in commercial 3D laser scanning systems for registration purposes and quality assurance [3]. The iterative closest point (ICP) approach is applicable under some specific circumstances for registering point cloud [4, 5].

Without using any accessory such as targets, this paper proposes a semi-automatic method for registration purposes. It considers some properties of LIDAR points as follows.

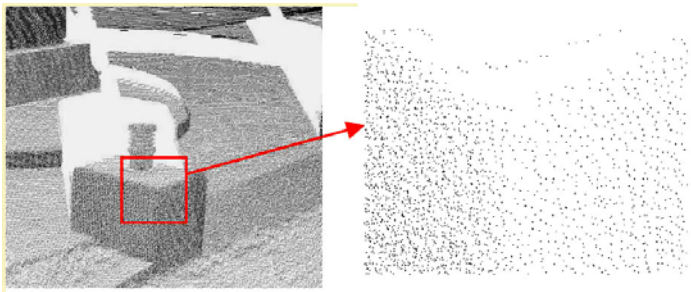

Fig. 1 difficulty on determining an exact corner point center visually by human vision.

2. Some Properties of LIDAR Points

3D laser scanner distributes LIDAR points in a sub-random manner [6]. Any two stations don't have a common scanned point. Also, LIDAR points are seldom (or always not) located exactly on interest features of scanned object surfaces. Moreover, global geometrical features of scanned objects are clear if LIDAR points are displayed in a 3D visualization system in a small scale. But, if LIDAR points are displayed in a larger scale, one almost cannot visually determine the exact feature center such as the corner feature point shown in Fig. 1, where the corner feature point is the intersection point of three planar polygons which intersect to each other near perpendicularly.

3. Key Ideas and the Method

To solve the above-mentioned problem, any corner feature point can be determined in a geometrical manner instead of manually. Firstly, a point cloud on a local plane is selected manually, and then a mathematical plane is fitted in a least squares manner onto them. Three local planes on an object corner are thus respectively determined, and their intersection point is computed by solving these three plane equations. Such points are used as tie points for transforming different laser coordinate systems into a common one. The transformation is bad in cases of inaccurate, or insufficient, or worse-distributed tie points. This paper adopts suitable "virtual corner points" to solve this problem. For details, please see the 5 and 6-th section. In the following sections, we are going to describe each step of the method in more details.

4. Least Squares Plane Fitting onto LIDAR Points

In order to determine an accurate 3D position of an interest corner feature point, a point cloud for each corresponding local planar polygon is selected manually in a visualization system, e.g. provided by the IMInspect module of the InnovMetric software used in our tests. Let x_i, y_i, z_i be the observations of 3D coordinates of a LIDAR point of the point cloud at a station, and v_x, v_y, v_z be their residuals, respectively. All points of a selected cloud are located on a local planar polygon and expressed in Eq. (1), where A~D are plane parameters.

$$A(x_i + v_x) + B(y_i + v_y) + C(z_i + v_z) + D = 0 \tag{1}$$

The Eq. (1) can be written as Eq. (2).

$$Ax_i + By_i + Cz_i + D = 0 + v_i \tag{2}$$

Those selected points are then fitted onto a mathematical plane expressed by the parameters A~D in a least squares manner, in which we let the sum of square perpendicular distances $\{d_i, \forall i\}$ of all selected points to the plane be minimal.

$$d_i d_i = \frac{(Ax_i + By_i + Cz_i + D)^2}{A^2 + B^2 + C^2} = \frac{v_i v_i}{A^2 + B^2 + C^2} \tag{3}$$

The Eq. (3) shows clearly that the above-mentioned criterion is identical to a minimal $\sum_i v_i v_i$ under the circumstance that A~C are constants for the plane. Let D be normalized to one. The observation equations are as follows, where the weight matrix P for all observations is assumed to be a unit matrix.

$$\begin{bmatrix} v_1 \\ v_2 \\ \vdots \\ v_n \end{bmatrix} = \begin{bmatrix} x_1 & y_1 & z_1 \\ x_2 & y_2 & z_2 \\ \vdots & \vdots & \vdots \\ x_n & y_n & z_n \end{bmatrix} \begin{bmatrix} A' \\ B' \\ C' \end{bmatrix} + \begin{bmatrix} 1 \\ 1 \\ \vdots \\ 1 \end{bmatrix} \qquad P = \begin{bmatrix} 1 & 0 & \cdots & 0 \\ 0 & 1 & \cdots & 0 \\ \vdots & \vdots & \ddots & \vdots \\ 0 & 0 & \cdots & 1 \end{bmatrix} \tag{4}$$

Let RMSD be the root mean square value of the perpendicular distances of all points in a least squares adjustment (LSA). Those points with $|v_i| > 3\text{RMSD}$ must be deleted, and in this case, a new LSA is computed. Repeat such process until all laser points with $|v_i| \leq 3\text{RMSD}$.

In our tests, about 1% of ground-based LIDAR points are deleted. If the scanning direction is (near) parallel to the plane, the deletion percentage increases to c.a. 10%. Moreover, about 1~5 LSA computations are needed to determine the final plane parameters. The shorter the scanning distance, the more LSA computations are needed.

The corner feature points are used as tie points for later registration purpose. The accuracy of each determined plane is a significant factor to the later registration. Therefore, the following three factors are to be studied.

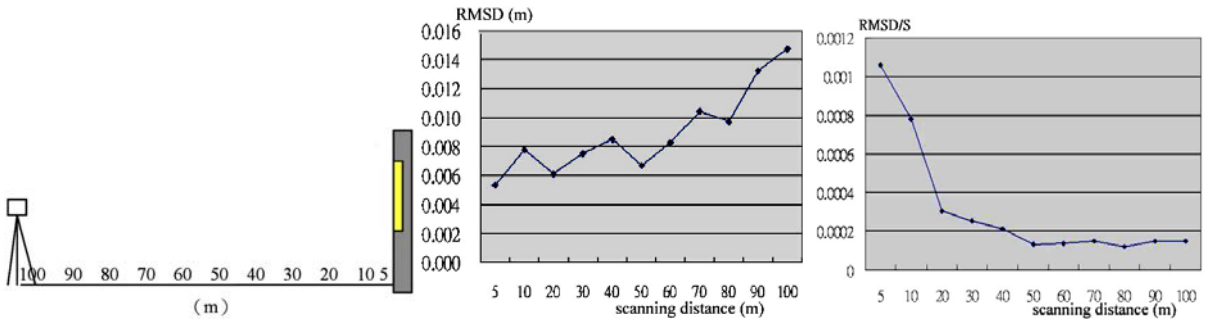

Fig. 2 a 3D laser scanner setup (left), fitting accuracy RMSD (middle), and the ratio of RMSD/S (right) at different scanning distance S from a flat wall.

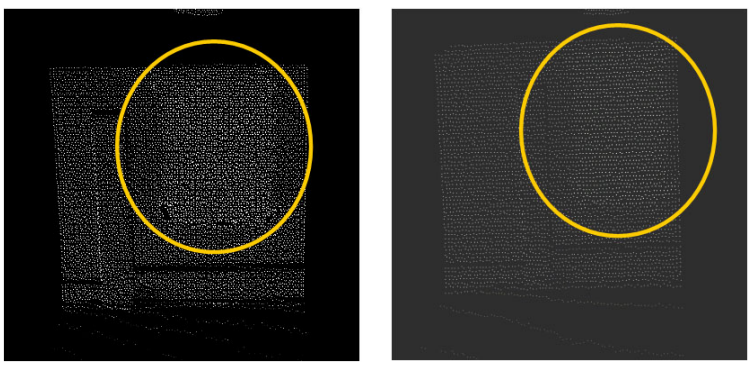

Fig. 3 difference of LIDAR intensities of points on two surface materials, namely paper and concrete, becomes smaller at a larger scanning distance S, e.g. S=40m (left) and S=60m (right).

1) scanning distance

In order to exam the relationship between the scanning distance S and the fitting accuracy RMSD, a 3D laser scanner is set up at different distance for S=5, 10, 20, …, 100m from a flat wall. The yellow area shown in Fig. 2 (left) denotes a white paper of the size 78.7cm × 109cm that is attached to that flat wall. Those laser points on that white paper can be differentiated from the others outside the paper area, because both groups have different intensity as shown in Fig. 3. Difference of LIDAR intensities of points on two materials, e.g. paper and concrete, becomes smaller at a larger scanning distance. It causes then difficulty on human interpretation and selection. The laser points on the white paper can be thus selected manually, and then fitted onto a mathematical plane in a least squares manner. Both the white paper and the wall are scanned by using the most fine scanning density, namely the scanning angle increment $\theta \cong 0.00016$ or one point per 2mm~16mm for S=5~100m. The fitting accuracy may be expressed by the afore-mentioned RMSD value. Fig. 2 (middle) shows clearly that the larger the scanning distance S is, the worse the fitting accuracy becomes. Nevertheless, the ratio RMSD/S converges approximately to a constant 0.00015 in cases of $S \geq 50$m. The constant 0.00015 is almost the same as the scanning angle increment $\theta \cong 0.00016$. It still should be further studied, whether both are correlated to each other.

2) point density

Furthermore, some more tests are done in order to exam whether the fitting accuracy is correlated to the point density. The 3D laser scanner is set up at different distances S=5, 20, 40, 60, 80 and 100m from the wall as shown in Fig. 2 (left). At the first three distances S=5, 20 and 40m, four different scanning densities (namely different LIDAR point spacing) are adopted. At the other three distances S=60, 80 and 100m, only three different scanning densities are used. The

relationship between the point density and the fitting accuracy is shown in Fig. 4. For S=5, 20 and 40m, RMSD ≅ 5~9mm, while the difference Δ of the RMSD values for different point densities at the same scanning distance S is about 0.15~0.5mm. Similarly for S=60, 80 and 100m, the RMSD values are 8~15mm and Δ≅0.7~1.4mm. In other word, the fitting accuracy (RMSD) is almost independent of the point density for a certain scanning distance.

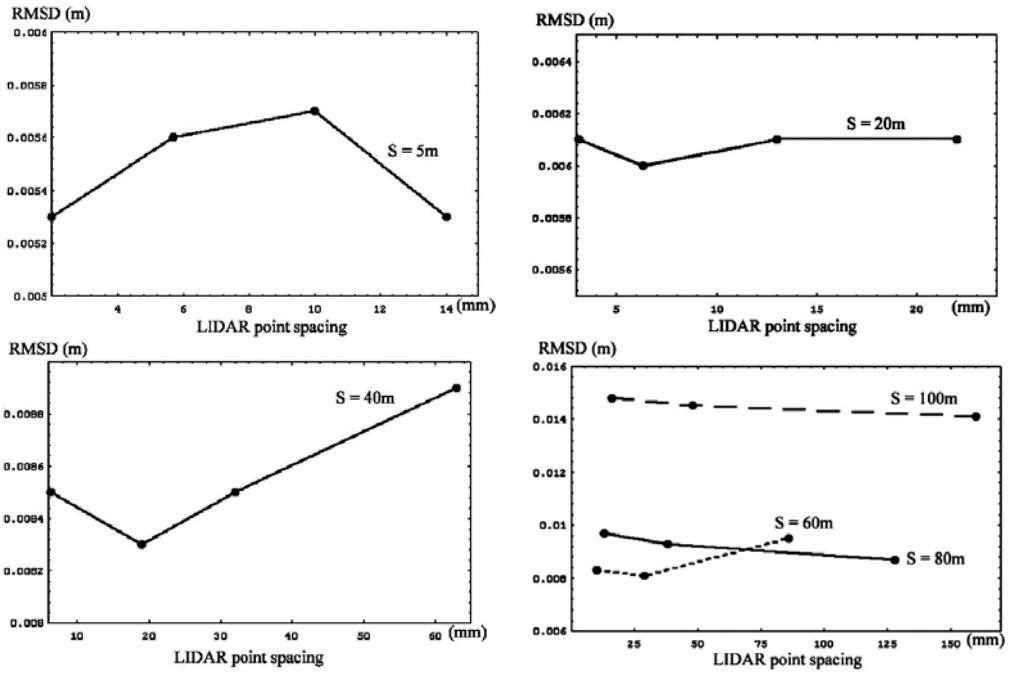

Fig. 4 relationship between the LIDAR point spacing and the fitting accuracy RMSD.

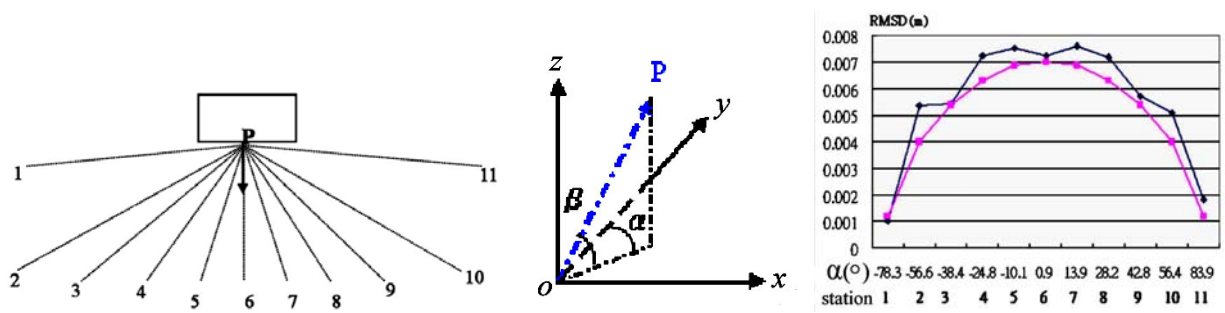

Fig. 5 horizontal relative positions between a scanned object and the scanning stations 1~11 (left), station coordinate system *xyz*, normal vector $\overrightarrow{OP}$ of the scanned object plane, α and β denote the horizontal and vertical angle of $\overrightarrow{OP}$ in the *xyz* system (middle), the relationship between the fitting accuracy RMSD and the scanning direction α (right).

3) scanning direction

Moreover, we want to see whether the fitting accuracy is correlated to the scanning direction. The experiments are done indoors in a classroom at NCKU in Taiwan. The scanned object is a table with the shape of a cuboid. Fig. 5 (left) shows the horizontal relative positions between the table and the scanning stations 1~11. Let *xyz* denote the 3D coordinate system at a scanning station. The normal vector of a scanned plane P on the table is expressed by $\overrightarrow{OP}$, while α and β, respectively, denote the horizontal and vertical angle of $\overrightarrow{OP}$ in the *xyz* system. All eleven stations almost have the same vertical scanning angle β (=-0.8°~+2.6°). The relationship between the fitting accuracy RMSD and the scanning direction α is illustrated in Fig. 5 (right), where ◆ denotes the LSA results, and ■ the product of cosα with the RMSD value at the station 6 with α=0.9°. Apparently, both curves are coincident with each other very well. In other word, the fitting accuracy RMSD is approximately proportional to cosα, where α is the angle between the scanning direction and the normal vector of the scanned plane. Furthermore, Fig. 6 illustrates the projection of 3D laser points scanned on the flat table plane onto the *xy*- (left) and *yz*-plane (right) in the station coordinate system. It shows clearly

that the laser points on the table edges have a significant larger deviation from the plane than the ones inside the table plane.

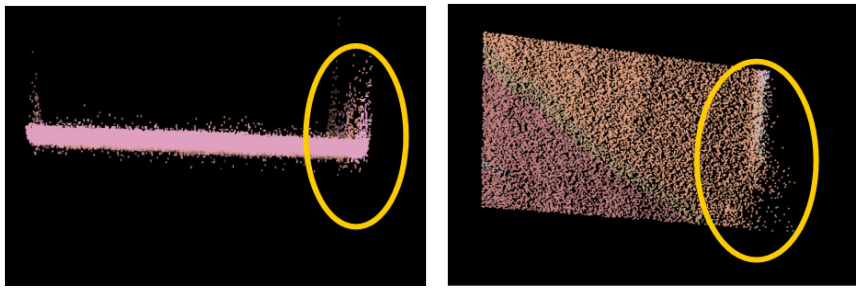

Fig. 6 projection of 3D laser points scanned on a flat table plane onto the *xy*- (left) and *yz*-plane (right).

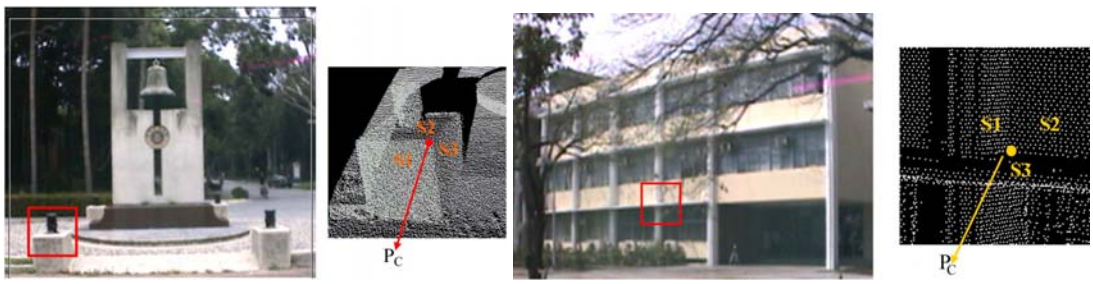

Fig. 7 an example of better (left) and worse (right) corner feature point in the NCKU campus.

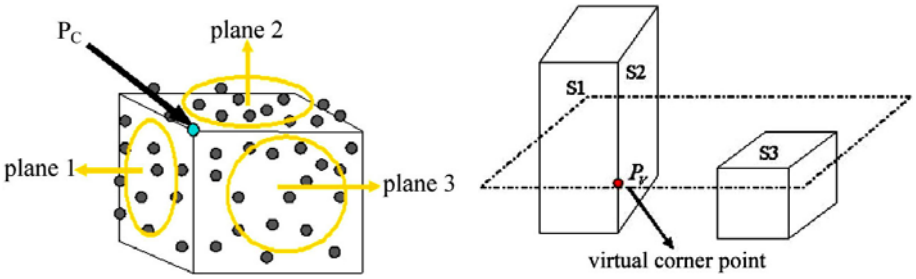

Fig. 8 intersection point P_C of three planes (left), virtual corner point P_V (right).

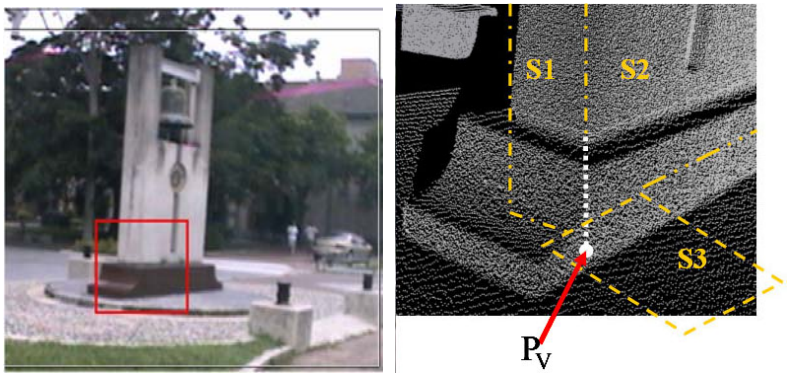

Fig. 9 an example of a virtual corner point P_V on the NCKU campus.

5. Intersection Point of Triple Planes

Now, three local planes on an object corner are thus respectively determined, and their intersection point (I.P.) is computed by solving these three plane equations. Such points are used as tie points for transforming different laser coordinate systems into a common one. Fig. 7 illustrates respectively an example of better (left) and worse (right) corner feature point P_C in the NCKU campus. The better P_C point is the I.P. of three nearly square planes with many uniformly distributed laser points. The other one is worse because the third plane S3 contains much less points due to occlusion. It

is clear to see that good 3D transformation needs well distributed tie points with good quality. If such requirement is not satisfied in practice, the so-called "virtual corner points" as shown in Fig. 8 (right) can be utilized to improve the geometrical configuration. The planar polygon S3 shown in Fig. 8 (right) may be either separated from the building containing the planes S1 and S2, or connected to that building while the region between S3 and the building is occluded. Fig. 9 illustrates an example of a virtual corner point on the NCKU campus. The accuracy of the extra-polated point P_V is unreliable and of course worse than the P_C point. Nevertheless, if the polygon S3 is not too far from the building, the error of the extra-polated 3D coordinates of the point P_V becomes insignificant if it is compared to the relative accuracy of local LIDAR points, e.g. expressed by the afore-mentioned RMSD value. Such virtual corner points should be then suitable for terrestrial LIDAR registration purpose.

6. Results of Registration Tests

After all corresponding tie points are determined in the above-mentioned operations, the 3D coordinate systems of all laser scanning stations are able to be transformed into a common one by using a 3D conformal transformation. The observation equation is expressed in Eq. (5), where (X_i^1, Y_i^1, Z_i^1) and (X_i^j, Y_i^j, Z_i^j) denote respectively the 3D coordinate observations of the *i*–th laser point at the first and *j*–th stations. The 3D coordinate system of the first station is used as the common reference one. All other stations are to be transformed into the reference system. No ground control points are used. The values $v_{X_i^j}, v_{Y_i^j}, v_{Z_i^j}$ are the residuals of the observations (X_i^j, Y_i^j, Z_i^j). R is the rotation matrix and λ denotes the scale factor. X_G, Y_G and Z_G are translation parameters. Both the horizontal coordinates of two good points at the first station and the vertical coordinates of three good points at the first station are fixed in the least square adjustment.

$$\begin{bmatrix} X_i^j + v_{X_i^j} \\ Y_i^j + v_{Y_i^j} \\ Z_i^j + v_{Z_i^j} \end{bmatrix} = \frac{1}{\lambda} R^T \begin{bmatrix} X_i^1 - X_G \\ Y_i^1 - Y_G \\ Z_i^1 - Z_G \end{bmatrix} \text{ with } R = \begin{bmatrix} \cos\Phi\cos K - \sin\Phi\sin\Omega\sin K & -\cos\Phi\sin K - \sin\Phi\sin\Omega\cos K & -\sin\Phi\cos\Omega \\ \cos\Omega\sin K & \cos\Omega\cos K & -\sin\Omega \\ \sin\Phi\cos K + \cos\Phi\sin\Omega\sin K & -\sin\Phi\sin K + \cos\Phi\sin\Omega\cos K & \cos\Phi\cos\Omega \end{bmatrix} \quad (5)$$

In the first iteration, the weight for each observation is given in Eq. (6), where $\bar{\sigma}$ denotes the average of the a posteriori standard deviations $\hat{\sigma}_X$, $\hat{\sigma}_Y$, $\hat{\sigma}_Z$ of all points.

$$p_X = \frac{\bar{\sigma}^2}{\hat{\sigma}_X^2} \qquad p_Y = \frac{\bar{\sigma}^2}{\hat{\sigma}_Y^2} \qquad p_Z = \frac{\bar{\sigma}^2}{\hat{\sigma}_Z^2} \quad (6)$$

In the later iterations, the weight is defined by the Eq. (6), if the absolute value of the residual is less than or equals $\bar{\sigma}$. Otherwise, the weight is given by Eq. (7).

$$p_X = \frac{\bar{\sigma}^2}{v_X^2} \qquad p_Y = \frac{\bar{\sigma}^2}{v_Y^2} \qquad p_Z = \frac{\bar{\sigma}^2}{v_Z^2} \quad (7)$$

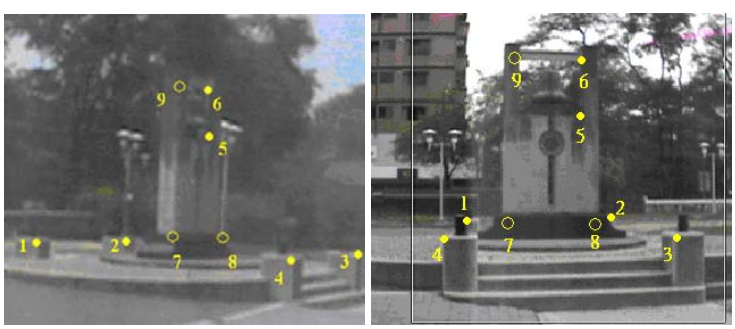

Fig. 10 two scanning stations and their corner points.

Fig. 10 illustrates two scanning stations and their corner points determined by the afore-mentioned operations, where the solid circles 1~6 are the corner feature points P_C, and the others 7~9 are the virtual corner points P_V. Fig. 11 shows the statistic figures of the test results. If only P_C points are used (case 1), the residual vector has in average a length of

1.4cm ($v_0 = \sqrt{v_X^2 + v_Y^2 + v_Z^2}$), while it increases to v_0 =3.3cm after introducing the virtual corner points 7~9 (case 2). The scale factors in the case 1 and 2 are λ=1.005±0.07 and λ=1.014±0.004, respectively. The accuracy of the related transformation parameters such as $\hat{\sigma}_\Phi$, $\hat{\sigma}_\Omega$ and $\hat{\sigma}_{ZG}$ is increased after the virtual corner points are applied.

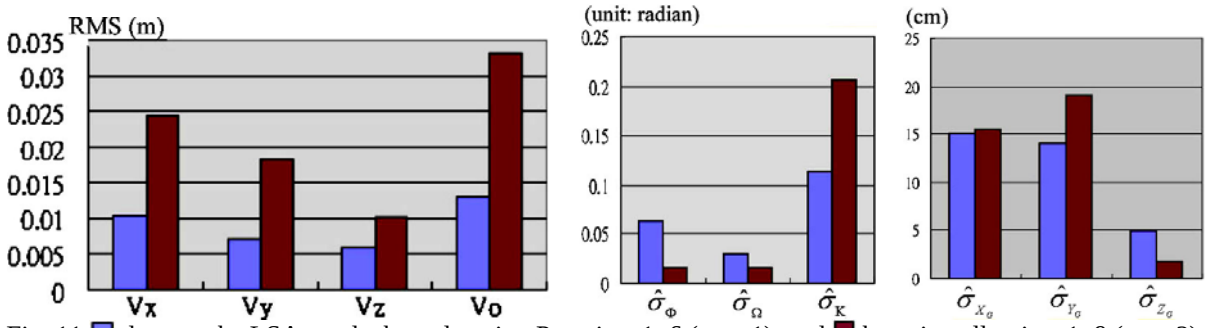

Fig. 11 ■ denotes the LSA results by only using P_C points 1~6 (case 1), and ■ by using all points 1~9 (case 2).

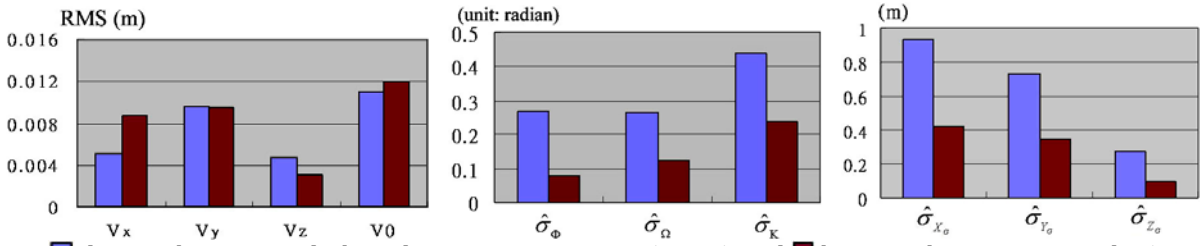

Fig. 12 ■ denotes the LSA results by only using P_C points 1~4 (case 3), and ■ by using the points 1~4 and 9 (case 4).

Fig. 12 shows the LSA results by only using P_C points 1~4 (case 3), and by using the points 1~4 and the virtual corner point 9 (case 4), where the four P_C points 1~4 are approximately co-planar. If only P_C points 1~4 are used (case 3), the residual vector has in average a length of v_0 =1.1cm, while it slightly increases to v_0 =1.2cm after introducing the virtual corner point 9 (case 4). The scale factors in the case 3 and 4 are λ=0.9998±0.200 and λ=1.0002±0.129, respectively. The accuracy of the translations parameters, namely $\hat{\sigma}_{XG}$, $\hat{\sigma}_{YG}$ and $\hat{\sigma}_{ZG}$, is ±0.29m~0.92m in the case 3. But it apparently increases to ±0.1m~0.42m after introducing the virtual corner point 9. Also, the accuracy of the rotation parameters, namely $\hat{\sigma}_\Phi$, $\hat{\sigma}_\Omega$ and $\hat{\sigma}_K$, is ±0.27~0.44 radian in the case 3. It increases to ±0.08~0.23 radian after using the virtual corner point 9. In other word, the test results show very clearly that suitable virtual corner points really can improve the geometrical condition for the transformation and thus raise the accuracy of corresponding transform parameters with the improvement rate of 36% to 71%.

Also, some more tests are done in order to exam the registration accuracy. No ground control points are used in the registration of LIDAR point clouds acquired at multiple ground-based laser scanning stations. Fig. 13 shows the relative positions of nine scanning stations around the building 1 on the NCKU campus, which is the building of the Department of Geomatics, NCKU. Fig. 14 illustrates the locations of the extracted corner feature points on the building 1 scanned at the stations 1-9 with different scanning distance and laser point spacing. Some points are the corner feature points P_C at certain stations, but they become virtual corner points P_V at the other neighbouring stations since they are occluded there. Fig. 15 expresses the *a posteriori* standard deviations of transformation parameters for the stations 2-9 in the open registration, where the coordinate system of the station 1 is used as the reference one, namely the common coordinate system after 3D conformal transformation for all nine stations. In that nine-station-registration, the 3D coordinates of the point 5 and 6 as well as the vertical coordinate of the point 2 in the station 1 are fixed. In other word, the points 5 and 6 as well as 2 are used as full and vertical reference points, respectively. It shows apparently that the *a posteriori* standard deviations of transformation parameters is proportional to the 5-7th power of the station number. Table 1 and 2 illustrate respectively the root mean square value of residuals v_X , v_Y and v_Z as well as residual vector length v_0 , and the *a posteriori* standard deviations of transformation parameters in the registration of any two contiguous stations with the first one as reference station. The registration may have a cm-level accuracy, if two contiguous stations have similar scanning direction and the same scanning distance as well as good configuration of tie points, e.g. the registration 1+2, 2+3, 4+5 and 8+9. Otherwise, the registration accuracy reaches a dm-level, e.g. the registration 3+4, 5+6, 6+7, and 7+8.

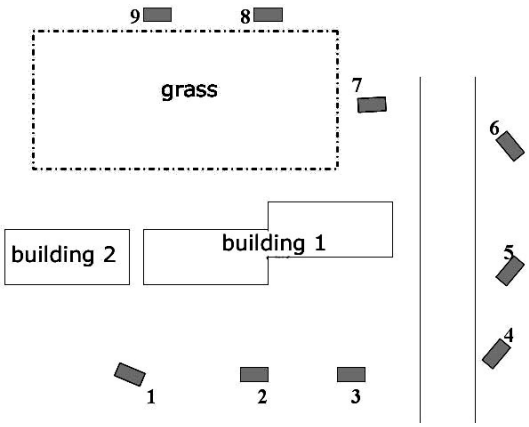

Fig. 13 the relative positions of nine scanning stations around the building 1 on the NCKU campus.

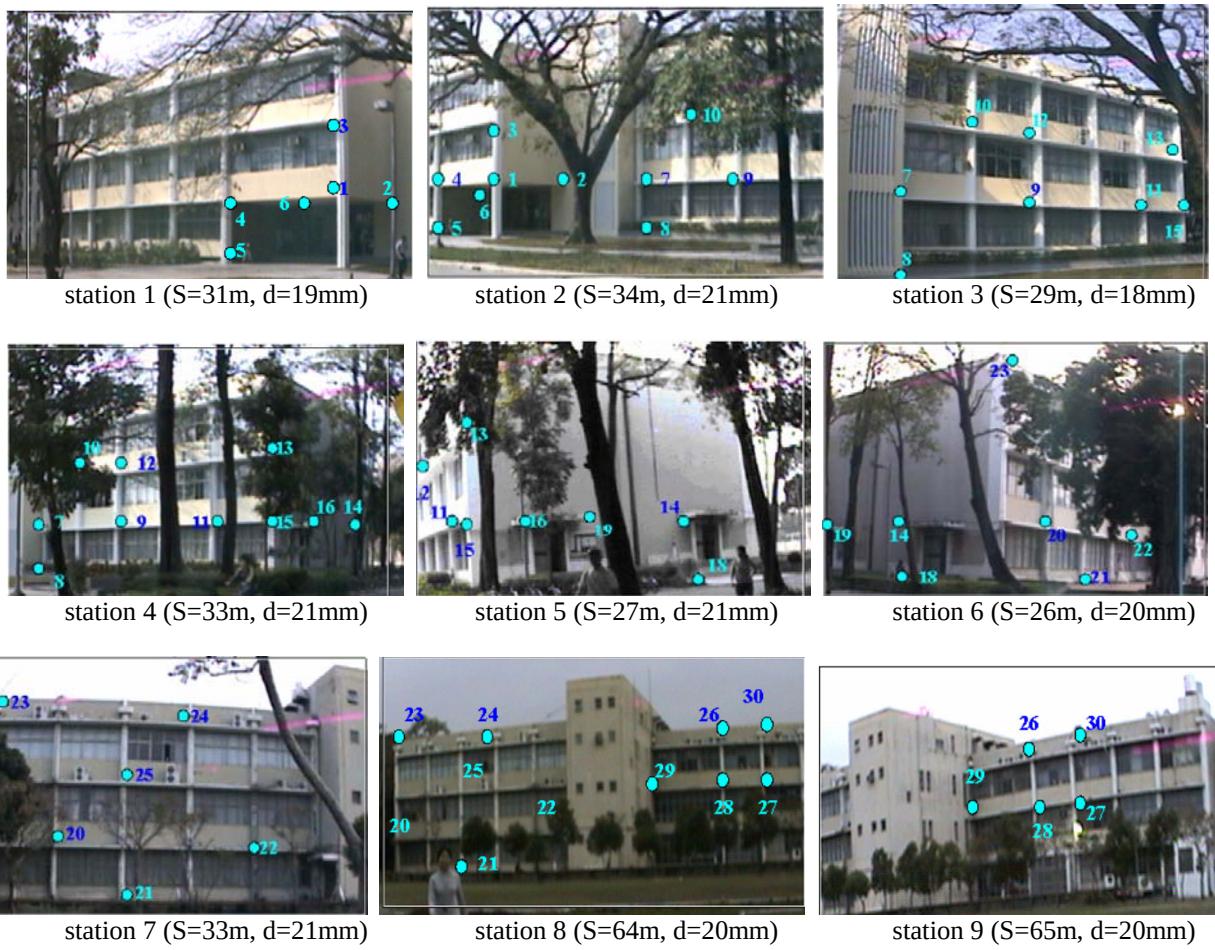

station 1 (S=31m, d=19mm) station 2 (S=34m, d=21mm) station 3 (S=29m, d=18mm)

station 4 (S=33m, d=21mm) station 5 (S=27m, d=21mm) station 6 (S=26m, d=20mm)

station 7 (S=33m, d=21mm) station 8 (S=64m, d=20mm) station 9 (S=65m, d=20mm)

Fig. 14 the extracted corner feature points on the building 1 scanned at the stations 1-9 with different scanning distance S and laser point spacing d.

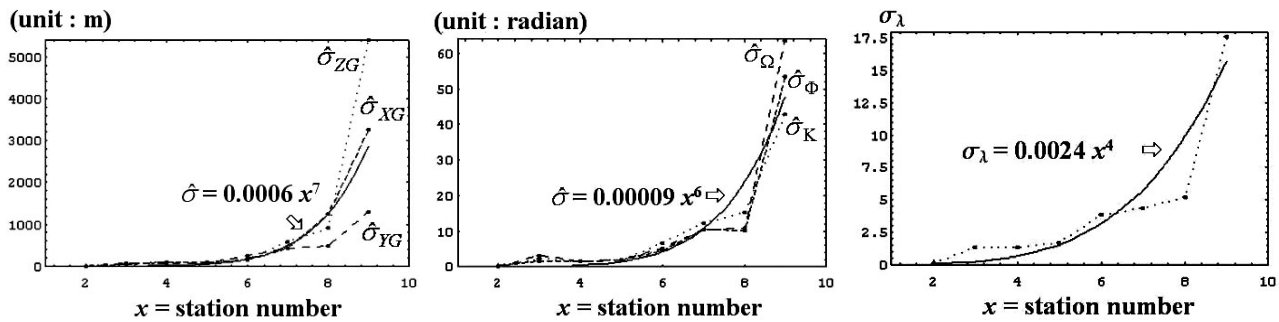

Fig. 15 the *a posteriori* standard deviations of transformation parameters for the stations 2-9 in the open registration with the reference station 1, where no ground control point is used.

Table 1 the root mean square value of residuals v_X, v_Y and v_Z as well as residual vector length v_0 in the registration of any two contiguous stations with the first one as reference station.

stations	RMS_ v_X (cm)	RMS_ v_Y (cm)	RMS_ v_Z (cm)	RMS_ v_0 (cm)
1+2	0.4	1.0	0.8	1.5
2+3	5.8	1.3	0.7	7.8
3+4	8.3	5.6	7.7	14.0
4+5	1.0	1.7	0.5	2.3
5+6	11.5	10.3	3.8	18.2
6+7	9.6	21.3	8.0	28.0
7+8	10.8	6.7	3.6	15.2
8+9	3.2	0.6	0.2	4.0

Table 2 the *a posteriori* standard deviations of transformation parameters in the registration of any two contiguous stations with the first one as reference station.

Stations	X_G (m)	Y_G (m)	Z_G (m)	Φ (radian)	Ω (radian)	K (radian)	λ
	$\hat{\sigma}_{XG}$ (m)	$\hat{\sigma}_{YG}$ (m)	$\hat{\sigma}_{ZG}$ (m)	$\hat{\sigma}_{\Phi}$ (radian)	$\hat{\sigma}_{\Omega}$ (radian)	$\hat{\sigma}_{K}$ (radian)	$\hat{\sigma}_{\lambda}$
1+2	15.638	-12.329	0.471	0.0026	-0.0511	-0.0577	1.0003
	0.042	0.033	0.049	0.0013	0.0010	0.0009	0.0006
2+3	13.138	-4.029	0.489	0.0043	0.0614	-0.0605	0.9956
	0.402	0.019	0.304	0.0017	0.0062	0.0072	0.0012
3+4	43.469	22.104	-16.031	-0.2978	0.1238	1.2140	1.0480
	26.605	51.614	23.219	0.5107	0.6945	1.0911	0.4175
4+5	24.350	15.792	-1.627	-0.1125	-0.0067	0.5475	1.0023
	0.580	0.694	0.532	0.0101	0.0171	0.0196	0.0156
5+6	37.213	24.283	3.570	0.0660	-0.1357	1.0621	0.9636
	193.485	459.939	270.049	4.8707	10.3060	13.2432	5.3742
6+7	37.703	12.045	-1.601	-0.0401	-0.0539	0.8318	0.9646
	14.407	15.789	27.670	0.5564	0.3963	0.4793	0.1111
7+8	42.591	-20.105	0.273	-0.0636	0.0034	0.4439	0.9866
	1.558	1.270	1.944	0.0077	0.0283	0.0255	0.0058
8+9	32.008	5.360	-0.514	-0.0397	-0.1097	0.1798	1.0006
	0.207	0.163	0.440	0.0028	0.0067	0.0034	0.0016

7. Concluding Remarks

This paper proposes a semi-automatic method for registration of terrestrial laser point sets acquired at different stations. The registration results may be worse in cases of inaccurate, or insufficient, or worse-distributed tie points. This paper adopts suitable "virtual corner points" to solve this problem.

The test results show some concluding remarks as follows:

1. The larger the scanning distance S is, the worse the fitting accuracy RMSD becomes. Nevertheless, the ratio RMSD/S converges approximately to a constant 0.00015 in cases of S≥50m, where RMSD denotes the root mean square value of the perpendicular distances from laser points to the corresponding plane. The constant 0.00015 is almost the same as the scanning angle increment θ≅0.00016. It still should be further studied, whether both are correlated to each other.
2. The fitting accuracy (RMSD) is almost independent of the point density for a certain scanning distance.
3. The fitting accuracy (RMSD) is approximately proportional to cosα, where α is the angle between the scanning direction and the normal vector of the scanned plane.
4. Suitable virtual corner points really can improve the geometrical condition for the transformation and thus raise the accuracy of corresponding transform parameters with the improvement rate of 36% to 71%.
5. The open two-station-registration may have a cm-level accuracy, if two contiguous stations have similar scanning direction and the same scanning distance as well as good configuration of tie points, e.g. the registration 1+2, 2+3, 4+5 and 8+9. Otherwise, the registration accuracy only reaches a dm-level, e.g. the registration 3+4, 5+6, 6+7, and 7+8.
6. In the open nine-station-registration, the *a posteriori* standard deviations of transformation parameters is proportional to the 5-7th power of the station number.

Acknowledgement

We sincerely appreciate the National Science Council at Executive Yuen, R.O.C. for supporting this work under the project numbers NSC93-2211-E-006-067.

References

[1] Zhao, H. and R. Shibasaki, 2001. A Robust Method for Registering Ground-based Laser Range Images of Urban Outdoor Objects, *Photogrammetry Engineering and Remote Sensing*, 67(10): 1143-1153.

[2] Dold, C. and C. Brenner, 2004. Automatic Matching of Terrestrial Scan Data as A Basis for The Generation of Detailed 3D City Models, *International Archives of Photogrammetry, Remote Sensing and Spatial Information Sciences*, Istanbul, Vol. 35, pp.1091-1096.

[3] **URL:** 3D laser scanning technology and its applications on engineering surveying. Written in Chinese by Tseng, Y.H. and T.Y. Shih. Available at: http://nhmrc.cv.nctu.edu.tw/People/tyshih/Publications/35.pdf.

[4] Besl, P. J. and N.D. McKay, 1992. A method for registration of 3-D shapes. *IEEE Transactions on Pattern Recognition and Machine Intelligence*, 14(2), pp. 239–256.

[5] Park J. and G. N. DeSouza, 2004. 3D Modeling of Real-World Objects Using Range and Intensity Images, (Book Chapter) Innovations in Machine Intelligence and Robot Perception, edited by: S. Patnaik, L.C. Jain, G. Tzafestas and V. Bannore, Springer-Verlag, pp.1-45.

[6] Axelsson, P., 1999. Processing of Laser Scanner Data—Algorithms and Applications. *ISPRS Journal of Photogrammetry & Remote Sensing*, 54: 138–147.